Harnessing Machine Learning and Physiological Knowledge for a Novel EMG-Based Neural-Machine Interface

Joseph Berman, Robert Hinson, I-Chieh Lee, and He Huang, *Senior Member, IEEE*

Abstract*—*Objective: **In this study, we aimed to develop a novel electromyography (EMG)-based neural machine interface (NMI), called the Neural Network-Musculoskeletal hybrid Model (N2M2), to decode continuous joint angles. Our approach combines the concepts of machine learning and musculoskeletal modeling.** ***Methods:*** **We compared our novel design with a musculoskeletal model (MM) and 2 continuous EMG decoders based on artificial neural networks (ANNs): multilayer perceptrons (MLPs) and nonlinear autoregressive neural networks with exogenous inputs (NARX networks). EMG and joint kinematics data were collected from 10 non-disabled and 1 transradial amputee subject. The offline performance tested across 3 different conditions (i.e., varied arm postures, shifted electrode locations, and noise-contaminated EMG signals) and online performance for a virtual postural matching task was quantified. Finally, we implemented the N2M2 to operate a prosthetic hand and tested functional task performance.** ***Results:*** **The N2M2 made more accurate predictions than the MLP in all postures and electrode locations ($p < 0.003$). For estimated MCP joint angles, the N2M2 was less sensitive to noisy EMG signals than the MM or NARX network with respect to error ($p < 0.032$) as well as the NARX network with respect to correlation ($p = 0.007$). Additionally, the N2M2 had better online task performance than the NARX network ($p \leq 0.030$).** ***Conclusion:*** **Overall, we have found that combining the concepts of machine learning and musculoskeletal modeling has resulted in a more robust joint kinematics decoder than either concept individually.** ***Significance:*** **The outcome of this study may result in a novel, highly reliable controller for powered prosthetic hands.**

***Index Terms*—Artificial neural network, electromyography (EMG), musculoskeletal model, neural machine interface, reinforcement learning.**

I. Introduction

OVER the past decades, research in electromyography (EMG)-based neural machine interfaces (NMI) has greatly advanced and been successfully applied to different machines, such as robots [1], [2], computer or virtual reality [3], [4], and multifunctional prosthetic arms [5], [6]. Focusing on robotic prostheses, EMG pattern recognition is one of commonly used decoding concepts that classifies multi-channel EMG signals into discrete motion types, such as hand open/close [7], [8], [9], [10], [11], [12], [13]. However, this approach can only operate one degree of freedom (DOF) at a time, producing non-natural prosthesis motions during functional task performance.

To enable natural, multi-joint coordinated prosthetic arm motion, recent research has focused on developing continuous EMG-based NMI for multifunction robotic prostheses. Existing continuous decoding algorithms can be divided into two categories: machine learning methods and musculoskeletal modeling approaches. In machine learning-based approaches, EMG signals are mapped directly to joint kinematics in a black-box style. The types of machine learning models used for these approaches range from linear regression [14], [15], [16] to artificial neural networks (ANNs) [15], [16], [17], [18], [19]. Machine learning approaches are entirely data-driven, requiring little prior knowledge of the physiology of the upper limb. However, these approaches can lack robustness to deviations in the input data from the original training data [17], [20], [21]. Another recent concept is deciphering EMG signals to estimate user intent based on the known physiology of human neural control of movements. From this concept, the EMG-driven musculoskeletal model-based approaches have been developed and tested [16], [22], [23], [24], [25], [26], [27], [28], [29]. Musculoskeletal models have incorporated deterministic components, such as Hill-type muscle models and multi-linkage arm dynamic models, to explicitly define the physiological mapping from EMG signals (efferent neural signals) to an internal muscle force state and the intended motion of the joints. This model-based approach has allowed EMG-based decoding to remain robust to variations in the input.

Manuscript received 23 April 2022; revised 20 July 2022 and 2 September 2022; accepted 26 September 2022. Date of publication 29 September 2022; date of current version 21 March 2023. This work was supported in part by NSF under Grant 1856441. *(Corresponding author: He Huang).*

Joseph Berman is with the Department of Electrical and Computer Engineering, North Carolina State University, USA, and also with the UNC/NC State Joint Department of Biomedical Engineering, North Carolina State University, USA.

Robert Hinson and I-Chieh Lee are with the UNC/NC State Joint Department of Biomedical Engineering, North Carolina State University, USA, and also with the University of North Carolina at Chapel Hill, USA.

He Huang is with the UNC/NC State Joint Department of Biomedical Engineering, North Carolina State University, Raleigh, NC 27695-7115 USA, and also with the University of North Carolina at Chapel Hill, Chapel Hill, NC 27599 USA (e-mail: hhuang11@ncsu.edu).

This article has supplementary downloadable material available at https://doi.org/10.1109/TBME.2022.3210892, provided by the authors.

Digital Object Identifier 10.1109/TBME.2022.3210892

Motivated by the complementary benefit of existing machine learning and neuromusculoskeletal modeling methods, in this study, we propose to combine the two concepts together to leverage their benefits for EMG-based neural interface design. Our present method still follows human physiology for movement production (i.e., EMG signals are mapped to joint torque which drives joint motion). However, our approach replaces the Hill-type muscle model with an ANN to map EMG signals to an internal state value we defined as virtual joint torque intended to drive a forward dynamics model to accurately estimate joint motion. One challenge for this approach is in training the ANN that maps EMG signals to virtual joint torque. This is because direct measurement of joint torque is difficult and impractical for daily use. One potential solution is to use inverse dynamics with the recorded motion to obtain values of joint torque. However, this method suffers from computational inaccuracies. Reinforcement learning (RL) is another potential solution to train the EMG decoding ANN. RL is an advanced form of machine learning [30] that allows agents to learn to take actions (prosthesis control) based on the human-prosthesis system state (i.e., EMG signals) to maximize a predefined reward function (i.e., the closeness of measured and estimated joint positions). Hence, RL can allow an ANN to be trained with a reward function based on the actual and estimated joint motions without the need for explicitly defining ground truth torque values.

Therefore, the goal of this study was to develop a novel framework for an EMG-based NMI that combines the concepts of machine learning and musculoskeletal modeling and can continuously identify the user's intended joint motion, which we refer to as the N2M2 decoder in this study. RL was used to train the N2M2 decoder. This system was evaluated offline and online with a real-time virtual postural matching task, as a comparison with the often-investigated continuous EMG decoders, including 1) a musculoskeletal model (MM), 2) a non-recurrent multi-layer perceptron (MLP), and 3) a recurrent ANN called a nonlinear autoregressive neural network with exogenous inputs, or NARX network (NN). In addition, we preliminarily demonstrated the physical task performance of prosthesis users, wearing a transradial prosthesis that was operated by our presented EMG-based neural interface. The contributions of this study include 1) a novel concept and framework for EMG decoding, 2) a pilot evaluation of performance and comparison with commonly reported musculoskeletal modeling and machine learning approaches to EMG decoding, and 3) implementation of the concept in real-time prosthesis control. The outcome of this study may lead to a novel design of a robust EMG-based NMI that can accurately predict both virtual joint torque and joint position. This study expands on our preliminary version of this concept [31].

II. Methods

A. Subjects

For this study, 10 non-disabled (ND) subjects (6 male, 4 female, ages 19-32, right-hand dominant) and 1 subject (male, age 42) with a right transradial amputation (TRA) sustained approximately 2 years prior to data collection were recruited.

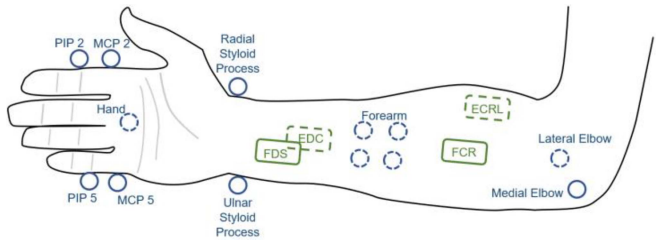

Fig. 1. Diagram of EMG electrode (green) and retro-reflective marker (blue) locations. Dashed lines indicate placement on the posterior section of the arm. PIP 2/5 = proximal interphalangeal joint of the 2nd and 5th digit; MCP 2/5 = metacarpophalangeal joint of the 2nd and 5th digit; ECRL = extensor carpi radialis longus; EDC = extensor digitorum communis; FCR = flexor carpi radialis; FDS = flexor digitorum superficialis.

Our experimental protocol was approved by the University of North Carolina at Chapel Hill Institutional Review Board and all subjects provided informed consent before participating.

B. Data Acquisition

First, the right forearm of each subject was cleaned with an alcohol pad. Then, 4 dry bipolar surface electrodes (SX230, Biometrics Ltd., U.K.) (material: steel, contact diameter: 10 mm diameter, contact spacing: 20 mm, CMRR @ 60 Hz: >96 dB, bandpass: 20–450 Hz) were placed over four muscles in the forearm which were identified by palpation: a) extensor carpi radialis longus (ECRL), b) extensor digitorum communis (EDC), c) flexor carpi radialis (FCR), and d) flexor digitorum superficialis (FDS). Thirteen retro-reflective markers were placed on the hand and forearm. For the TRA subject, we placed the markers on the intact upper limb for mirrored bilateral movements to be conducted. The locations of the electrodes and markers are shown in Fig. 1. Electrodes were connected to an amplifier (K800 Amplifier, Biometrics Ltd. U.K.) and EMG signals were recorded at 1000 Hz while the 3-dimensional positions of each marker were recorded at 100 Hz by an infrared motion capture system (Vicon Motion Systems Ltd. U.K.) (typical error <1 mm). The EMG system was connected to the analog-to-digital interface of the motion capture system to synchronize the data.

We first collected EMG data while subjects performed the maximum voluntary contraction (MVC) for flexion and extension of both the wrist and MCP joints. Subjects were then instructed to perform movements of the wrist and MCP joints in either a cyclical pattern or in self-selected velocities. For patterned movements, subjects began in a neutral position with their joints between fully flexed and fully extended positions and their muscles relaxed. The pattern involved moving the targeted joint between the neutral, fully flexed, neutral, and fully extended positions at a 0.25 Hz rate set on a metronome. For each posture, subjects performed 5 movement types: 1) isolated wrist flexion/extension in a pattern, 2) isolated MCP flexion/extension in a pattern, 3) isolated wrist flexion/extension in self-selected velocities, 4) isolated MCP flexion/extension in self-selected velocities, and 5) simultaneous wrist and MCP flexion/extension in self-selected velocities. For all MCP joint movements, subjects were instructed to keep their 4 fingers

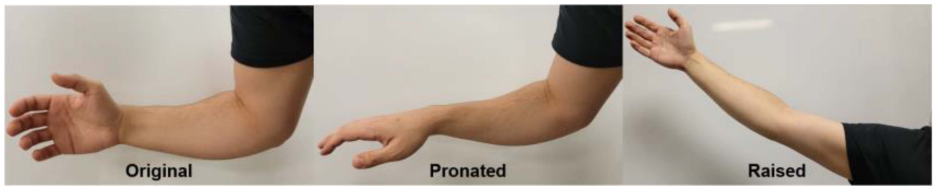

Fig. 2. The three tested arm postures for offline decoder evaluation.

together throughout the trial and move them all simultaneously. Subjects rested between trials to reduce muscle fatigue. For ND subjects, EMG and kinematic data were collected in 3 different postures: original, pronated, and raised (Fig. 2). These postures were chosen to reflect commonly used postures in activities of daily living (ADLs), each of which are affected differently by gravity. In the original posture, 2 trials lasting approximately 30 s each were completed for each movement type for a total of 10 trials. One trial for each movement type was randomly selected to train each decoder while the other trials were reserved to test performance. In the other 2 postures 1 trial lasting approximately 30 s was completed for each movement type for a total of 5 trials in each posture. After all trials were completed, the location of each electrode was marked on the subject's forearm. Then, each electrode was moved 0.5 cm perpendicular to the muscle fibers. The ND subjects were then instructed to reperform the 5 trials in the original posture only. The TRA subject completed 2 trials lasting approximately 30 s for each movement type in the original posture only.

C. Simulated Noise

In addition to the varied posture and shifted electrode data, we created a third set of testing data by simulating a noisy EMG signal. This was done by adding white, zero-mean Gaussian noise with varying standard deviations to the raw EMG signals from the original posture testing data trials of ND subjects. The recorded values of the raw EMG signals were typically within the range of -1 V to 1 V. Thus, we investigated simulated noise cases with standard deviations in a relatively moderate range of 0 to 0.010 V incremented in steps of 0.001 V as this was found to be sufficient to observe performance drops.

D. Data Processing

Muscle activation levels were estimated from the mean absolute value (MAV) of the EMG signals obtained using a 100 ms sliding window adjusted in 10 ms increments, resulting in processed EMG signals with a frequency of 100 Hz to match the frequency of the marker position data. The maximum values of the processed EMG signals from the MVC trials were used to normalize the EMG data from all other trials. Marker positions were low-pass filtered using a 4th-order Butterworth filter with a cutoff frequency of 5 Hz similar to previous studies [20], [22], [27]. Wrist and MCP joint angles were calculated from filtered marker positions using inverse kinematics. The processed data from 1 trial for each of the 5 movement types in the original posture were randomly chosen as training data. The remaining trials were reserved as testing data to validate the performance of each decoder.

E. Multilayer Perceptron Decoder

Multilayer perceptrons (MLPs) were created using the Deep Learning Toolbox in MATLAB 2021a (Mathworks Inc., USA). A separate MLP was created for each of the 2 joints for each subject and was trained to map processed EMG signals directly to joint angles. Each MLP was trained until performance no longer significantly increased (i.e., the gradient of normalized mean squared error fell below 10e-8). To obtain maximum performance, we tested the MLPs as we incremented the number of neurons in the hidden layer and then the number of hidden layers used until we no longer observed a significant increase in performance. The final structure contained 1 hidden layer with 5 neurons.

F. NARX Network Decoder

Nonlinear autoregressive neural networks with exogenous inputs, or NARX networks (NNs), were created using the Deep Learning Toolbox in MATLAB 2021a. An NN is a special type of recurrent neural network that predicts values in a time series based on previous values from the time series, which has previously shown success in EMG-based decoding of kinematics [32]. The input to the NN included processed EMG signals with no time delay in addition to the joint angle from the previous timestep. NNs were first trained in an open-loop configuration in which input joint angles were ground-truth values taken from the training data. Training completed when performance no longer significantly increased as described above. Then the NARX network was switched to a closed-loop configuration in which the input joint angle was the joint angle predicted by the network with a time delay of 1 timestep. The NARX network was trained a second time in the closed-loop configuration until performance no longer significantly increased. We tested the NNs as we incremented the number of neurons in the hidden layer and then the number of hidden layers used until we no longer observed a significant increase in performance. The final structure also contained 1 hidden layer with 5 neurons. The final structure in open-loop and closed-loop configurations is shown in Fig. 3.

G. Musculoskeletal Model Decoder

A musculoskeletal model (MM) decoder containing 4 muscles modeled as Hill-type actuators with contractile elements and parallel elastic elements was defined in MATLAB. The 4 muscles included 2 agonist/antagonist pairs: 1 crossing the

TABLE I
MUSCULOSKELETAL MODEL PARAMETERS AND CONSTRAINT RANGES

Parameter	Constraint Range (Non-Disabled Subjects)	Constraint Range (Transradial Amputee Subjects)			
		ECRL	EDC	FCR	FDS
Optimal contractile element length, L_0^{CE} (m)	0.01 – 0.5	0.038 – 0.094	0.046 – 0.087	0.038 – 0.082	0.049 – 0.103
Maximum isometric contractile element force, F_0^{CE} (N)	10 – 1000	20 – 946.9	7.8 – 193.3	20.2 – 611.8	39.6 – 1317.1
Moment arm, wrist, ma_{wrist} (m)	0.001 – 0.05	0.001 – 0.02	0.011 – 0.014	0.01 – 0.026	0.008 – 0.022
Moment arm, MCP, ma_{MCP}* (m)	0.001 – 0.05	0 – 0	0.005 – 0.011	0 – 0	0.007 – 0.023
Contractile element length in neutral position, $L_{\theta=0}^{CE}$ (unitless)	$0.75L_0^{CE} - 1.25L_0^{CE}$	$0.75L_0^{CE} - 1.25L_0^{CE}$	$0.75L_0^{CE} - 1.25L_0^{CE}$	$0.75L_0^{CE} - 1.25L_0^{CE}$	$0.75L_0^{CE} - 1.25L_0^{CE}$
Passive elastic element stiffness (N/m^2)	10 – 200	0.5 – 1.1	0.5 – 1.1	0.5 – 1.1	0.5 – 1.1

*ma_MCP = 0 for ECRL and FCR.

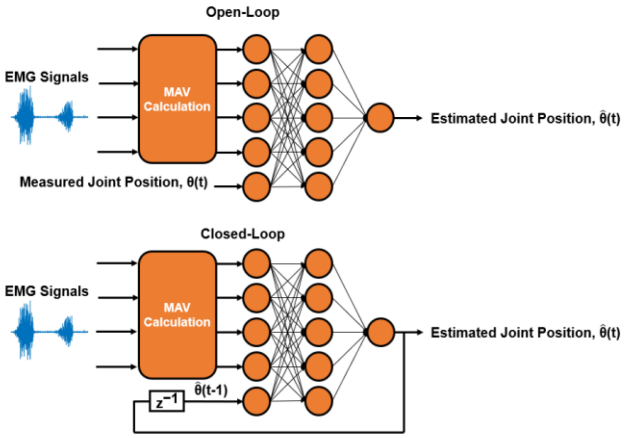

Fig. 3. Structures of the NARX network decoder in open-loop (top) and closed-loop (bottom) configurations. The decoder was calibrated first in open-loop and then in closed-loop configurations, but for real-time use, only the closed-loop configuration was tested.

wrist joint and 1 crossing the wrist and MCP joints. For each muscle, 6 parameters, each constrained to an approximate range of physiological values (Table I), were optimized using the GlobalSearch function from the Global Optimization Toolbox in MATLAB 2021a to minimize the mean squared error between measured and estimated joint angles. Individual constraints for each muscle chosen based on physiological values were found to work best for the TRA subject, but approximate ranges used across all muscles were found to work best for the ND subjects. Because the MCP joint has a smaller range of motion than the wrist joint, the values of squared errors calculated for the MCP joint were weighted twice as high as the squared errors calculated for the wrist joint. The inputs to the model were muscle activations approximated from processed EMG signals using the following functions:

$$u_k = \alpha E_{k-d} - \beta_1 u_{k-1} - \beta_2 u_{k-2} \tag{1}$$

$$a_k = \frac{e^{Au_k} - 1}{e^A - 1} \tag{2}$$

where E_k is the processed EMG signal at the current timestep k, d is the electromechanical delay equal to 4 (equivalent to 40 ms), and α, β_1, β_2, and A are coefficients equal to 1.1881, -0.18, 0.0081, and -1 respectively following the methods used in [16].

The force estimated by each muscle model was used to drive a forward dynamics model of the hand and wrist. Two segments representing the palm and fingers were defined as uniform solid

TABLE II
FORWARD DYNAMICS MODEL PARAMETERS

Parameter	Value
Mass of the palm, M_{palm} (kg)	0.90
Mass of the fingers, $M_{fingers}$ (kg)	0.70
Length of the palm, L_{palm} (m)	0.094
Length of the fingers, $L_{fingers}$ (m)	0.092
Damping coefficient of the wrist joint, c_{wrist} (Nms/rad)	0.60
Damping coefficient of the MCP joint, c_{MCP} (Nms/rad)	0.30
Limiting stiffness, K_{lim} (Nm/rad)	10
Limiting damping coefficient, c_{lim} (Nms/rad)	0.03

cylindrical rods and pin joints were used to represent the wrist and MCP joints. The moment of inertia for each segment was defined as

$$I = \frac{1}{3}ML^2 \tag{3}$$

where M and L are the mass and length of each segment respectively. Additionally, damping components were defined for both joints. Each parameter was predefined and used for all subjects. The mass and damping coefficient values were initially set within realistic physiological ranges but were each increased to improve the stability of the model. Lengths were based on the measured lengths of a researcher's palm and fingers. A spring-damper component was used to generate limiting forces when either joint moved outside of its respective range of motion (Wrist joint: [−90°, 90°]; MCP joint: [−5°, 88°]). The final parameters used are shown in Table II. The full details of the model are described in [22].

H. Neural Network-Musculoskeletal Hybrid Model Decoder

RL agents were created using the Reinforcement Learning Toolbox in MATLAB 2021a. The agents were implemented using the Deep Deterministic Policy Gradient (DDPG) algorithm. This algorithm uses an actor-critic ANN structure in which the actor network is trained to predict the optimal action given the current state and the critic network is trained to predict the long-term discounted reward given the current state and the action taken. The details of the DDPG algorithm are described in [33]. The actor network contained 2 hidden layers with 200 and 100 neurons. The critic network contained a path for the state input and a path for the action input each containing 2 hidden layers with 100 and 50 neurons which were combined

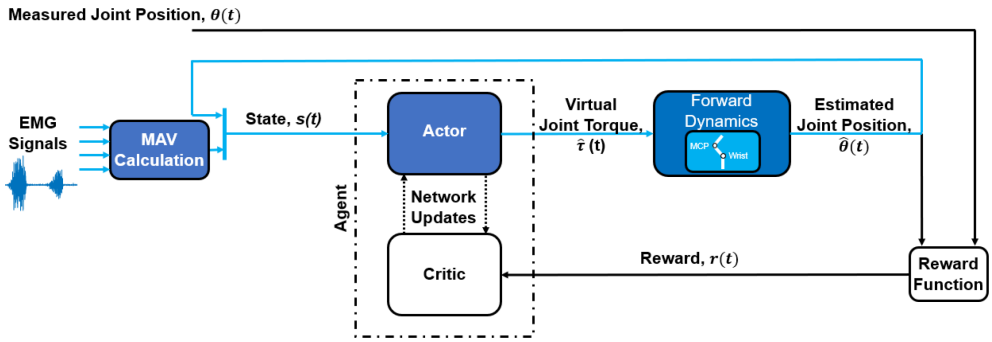

Fig. 4. Block diagram of the N2M2 decoder. Only the blue blocks and paths were active during real-time use. The measured joint positions, reward function, and critic were only active during calibration.

using an addition layer. All hidden layers used the rectified linear unit (ReLU) activation function and the output layer of the actor network also used a hyperbolic tangent (tanh) activation function followed by a scaling layer while the output layer of the critic network used no activation function. We defined the state as a vector with a length of 5 containing the 4 values of the processed EMG signals at the current timestep and the joint angle estimated in the previous timestep. We defined the action as a virtual joint torque value, $\hat{\tau}$, for the targeted joint. Temporally correlated noise was added to the virtual torque values during training to encourage action exploration as described in [33]. The virtual joint torque values were used as inputs to the same forward dynamics model used in the MM decoder. Multi-agent reinforcement learning (MARL) was used to allow agents for the wrist and MCP joints to be trained and provide inputs to the forward dynamics model simultaneously. Finally, to train the agents we defined our reward function based on [34]:

$$Reward = \frac{1}{\alpha + \left|\theta_k - \hat{\theta}_k\right|} \tag{4}$$

where θ_k is the measured joint angle in radians at timestep k, $\hat{\theta}_k$ is the estimated joint angle at timestep k, and α is a constant value. The full block diagram of the Neural Network-Musculoskeletal Hybrid Model (N2M2) decoder is shown in Fig. 4. We retrained and tested N2M2 decoders while increasing the value of α by 0.1 through a range of 0.1 through 1.0 as we found this range was sufficient to find a peak in average performance. Maximum average performance was found at $\alpha = 0.7$ for the wrist agents and $\alpha = 0.5$ for the MCP agents. All hyperparameters used with the DDPG algorithm were tuned using similar methods to maximize performance and are listed in Table III.

TABLE III
HYPERPARAMETERS USED WITH THE DEEP DETERMINISTIC POLICY GRADIENT ALGORITHM

Hyperparameter	Value
Learning Rate	1e-4
Experience Buffer Length	1e5
Discount Factor	0.95
Mini Batch Size	200
Target Update Frequency	1
Target Smoothing Factor	1e-3
Noise Variance (Wrist)	0.5
Noise Variance (MCP)	0.25
Noise Variance Decay Rate (Wrist)	1e-5
Noise Variance Decay Rate (MCP)	1e-5
Output Scaling Factor (Wrist)	2
Output Scaling Factor (MCP)	1

I. Offline Estimation Performance Metrics

Each trained decoder was used to estimate wrist and MCP joint angles for all testing data trials. Then to evaluate performance, we calculated Pearson's correlation coefficient (r) between measured and estimated joint angles:

$$r = \frac{\sum_{k=1}^{N}\left(\theta_k - \theta_{avg}\right)\left(\hat{\theta}_k - \hat{\theta}_{avg}\right)}{\sqrt{\sum_{k=1}^{N}\left(\theta_k - \theta_{avg}\right)^2}\sqrt{\sum_{k=1}^{N}\left(\hat{\theta}_k - \hat{\theta}_{avg}\right)^2}} \tag{5}$$

where θ_k and $\hat{\theta}_k$ are the k[th] measured and estimated joint angle respectively, θ_{avg} and $\hat{\theta}_{avg}$ are the mean measured and estimated joint angle respectively, and N is the total number of data points in the given trial. In addition, we calculated the normalized root mean squared error (NRMSE) defined as the root mean squared error between measured and estimated joint angles normalized by the total range of measured joint angles:

$$NRMSE = \frac{\sqrt{\frac{1}{N}\sum_{k=1}^{N}\left(\theta_k - \hat{\theta}_k\right)^2}}{\left(\theta_{max} - \theta_{min}\right)} \tag{6}$$

where θ_k and $\hat{\theta}_k$ are the k[th] measured and estimated joint angle respectively, θ_{max} and θ_{min} are the maximum and minimum measured joint angle, respectively, for the given trial, and N is the total number of data points in the given trial. For all 3 postures and both electrode locations, both Pearson's correlation coefficient and NRMSE suggested similar outcomes. Thus, for simplicity NRMSE is only reported for simulated noise cases.

Finally, the smoothness of the estimated trajectories of joint positions was quantified using the mean absolute value of the third derivative (i.e., jerk), or mean absolute jerk, averaged across all trials (excluding simulated noise cases):

$$Mean\ Absolute\ Jerk = \frac{1}{N}\sum_{k=1}^{N}\left|\frac{d^3}{dt^3}\hat{\theta}_k\right| \tag{7}$$

where $\hat{\theta}_k$ is the kth estimated joint angle and N is the total number of data points in the given trial. This metric was inspired by previous studies that used the third derivative to estimate the smoothness of motion [35] such as 1 study that used the integral of squared jerk to quantify the smoothness of patterns drawn by subjects with Parkinson's disease [36].

For trials that only included 1 actively moving joint, metrics are considered for that joint only. For trials that included both joints moving simultaneously, the metrics of both joints were considered.

J. Real-Time Control

To validate the feasibility of real-time control of a prosthetic device using our N2M2 decoder, we defined 4 tests: 1 virtual posture matching test displayed on a computer screen and 3 tests to be completed using a prosthesis. The prosthesis consisted of an active terminal device (MyoHand VariPlus Speed, Ottobock, Germany) connected to a wrist flexor and wrist rotator. An adapter was designed to mount the prosthesis to the upper limb of ND subjects while allowing flexion and extension of the elbow and natural wrist movements. The 3 tests using the prosthetic device include Box and Blocks, Modified Page Turning, and Modified Shelf tests. Each of these 3 tests were set up on a 73.7 cm tall table that subjects stood in front of. Each subject completed 5 trials for each test. Subjects completed the virtual hand test using both the N2M2 and NN decoders to establish a comparison. For simplicity, the MLP decoder was not considered for this test due to its significantly lower performance. All other tests using the physical prosthetic device were completed using the N2M2 decoder only to demonstrate the capabilities of the decoder for real-time control. The device allowed control of 3 DOF (hand open/close, wrist flexion/extension, and wrist pronation/supination). Encoders were mounted on the device for each DOF and a PID controller was tuned to allow for position-based control. Only the hand open/close and wrist flexion/extension DOF were actively controlled by subjects. The wrist was rotated to a predetermined position prior to each test (original for the Box and Blocks Test and pronated for the Modified Page Turning and Shelf tests).

Five of the 10 ND participants returned on a separate day to complete these tests. The forearms of all subjects were again cleaned with an alcohol wipe and 4 bipolar surface electrodes were placed in approximately the same original locations. Before beginning the tests, subjects were instructed to complete another MVC trial in which only EMG data were collected. These data were processed the same as previously described and used to normalize all EMG data recorded in real-time. Next, the inputs and outputs of the decoders were manually linearly scaled by experimenters, following the methodology of previous studies [24], [37], [38], to ensure the subject could comfortably reach all angles in the range of motion for each joint without excessive physical effort. In addition, to help improve the stability of the estimated joint angles for the virtual hand test only, moving average filters with window sizes equivalent to 80 ms were placed directly at the output of each decoder and the filtered output values were used in the feedback loops. Due to the natural lowpass filtering effect introduced by including a physical motor in the control loop, the moving average filter was found to provide little benefit and was not used for any of the other tests.

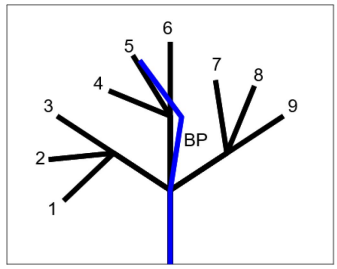

Fig. 5. The 9 target postures (black) and base posture (blue) in the online postural matching task.

1) Virtual Posture Matching Test: Subjects were seated in front of a monitor that displayed a 2-DOF planar link-segment virtual hand based on the setups from previous studies [13], [24], [37], [38], [39], [40] which visualized the joint angles estimated by the decoder. Subjects were asked to move the virtual hand from a base posture to each of the 9 target postures (Fig. 5) as they appeared. After each target posture was reached, subjects relaxed their hand and returned the virtual hand to the base posture. Target postures were considered completed when both joints were held within $\pm 5°$ of the target posture for 0.5 consecutive seconds. The base posture was considered completed when both joints were held within $\pm 8°$ of the base posture for 0.25 consecutive seconds. The displayed posture turned green to indicate the virtual hand was within the required range. The order the target postures appeared in was randomized for each subject and subjects were given 60 s to hit each target posture. Subjects were allowed to practice with each decoder to familiarize with the test and allow experimenters to adjust the linear scaling prior to recorded trials. The decoder used first was randomized for each subject and subjects were blinded to which decoder they were using during the trials. Subjects completed 5 trials using each decoder.

The performance metrics used in this test were task completion percentage, defined as the number of target postures successfully completed in the given 60 s, task duration, defined as the time taken to hit the target postures when starting from the base posture, number of overshoots, defined as the number of times the virtual hand moved in and out of the required range of the target posture, and normalized path length, defined as the length of the angular trajectory taken by the virtual hand normalized by the length of the minimum angular trajectory between the base posture and target posture:

$$Normalised\ Path\ Length = \frac{\sum_{k=1}^{N-1}\sqrt{\left(\theta_{k+1}^{w}-\theta_{k}^{w}\right)^{2}+\left(\theta_{k+1}^{m}-\theta_{k}^{m}\right)^{2}}}{\sqrt{\left(\theta_{t}^{w}-\theta_{i}^{w}\right)^{2}+\left(\theta_{t}^{m}-\theta_{i}^{m}\right)^{2}}} \quad (8)$$

where θ_k^w and θ_k^m are the kth wrist and MCP joint angles of the virtual hand, θ_t^w and θ_t^m are the wrist and MCP joint angles of the target posture, θ_i^w and θ_i^m are the initial wrist and MCP joint angles, and N is the total number of data points in the given trial. Task duration, number of overshoots, and normalized path length

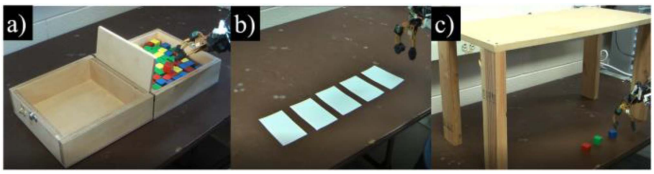

Fig. 6. The Box and Blocks Test (a), Modified Page Turning Test (b), and Shelf Test (c).

were only considered for successfully reached target postures. Additionally, to quantify the smoothness of the estimated joint positions for each trial, the mean absolute jerk was calculated as previously described.

Finally, after all trials were completed but before revealing the order of the decoders, subjects were asked which decoder they preferred using in terms of quickly and efficiently reaching all postures.

2) Box and Blocks Test: A common test for measuring functional ability in the upper limb is the Box and Blocks Test [41]. The test consists of a 53.7 cm by 25.4 cm wooden box separated into 2 equal sections by a 15.2 cm tall partition (Fig. 6(a)). One hundred and fifty blocks with 2.5 cm long sides were placed on the right side of the partition. Subjects stood in front of the box and were given 60 s to move as many blocks as they could from the right side of the partition to the left. For a block to be counted, the terminal device of the arm was required to cross the partition. If multiple blocks were successfully transported in 1 movement, only 1 was counted.

3) Modified Page Turning Test: Page turning is a test included in the Southampton Hand Assessment Procedure [42]. The original test involves a card placed on a table which subjects are asked to flip horizontally to simulate turning the pages of a book. This test can be used to evaluate functionality of forearm pronation/supination in a prosthetic arm. For our modification, to demonstrate control of the wrist flexion/extension DOF, subjects were instructed to flip cards by instead grasping the card and using a wrist flexion motion to flip the card vertically. Five 3 in by 5 in index cards were placed on a Table I in apart from each other and 5 in from the edge of the table (Fig. 6(b)). The time taken by the subject to flip all 5 cards was recorded.

4) Shelf Test: To further demonstrate the simultaneous control of the hand open/close and wrist flexion/extension DOF in addition to the robustness of the N2M2 decoder for a raised arm posture, we defined 1 additional test. Subjects stood in front of a table with an 45.7 cm tall wooden bench placed on top to simulate a shelf (Fig. 6(c)). Three blocks used in the Box and Blocks Test were placed on the table under the bench. Subjects were given 60 s to move the blocks 1 at a time back and forth between the table (lower level) and the top of the bench (higher level). All 3 blocks were required to be moved to the next level before any could be moved back. Subjects were allowed to use their left hand to readjust any of the blocks if they landed in a position difficult to reach with the arm. If a block dropped to the floor, the subject was instructed to move on to the next block while an experimenter retrieved the dropped block. The total number of blocks moved from 1 level to another was recorded.

K. Data Analysis

1) Offline Estimation Performance: To evaluate the robustness of decoders, the results of correlation coefficient (r) and NRMSE were used to compare the decoders at varied postures (4 decoders (N2M2, MM, NN, and MLP) X 3 arm postures (original, pronated, and raised)) and decoders with different electrode locations (4 decoders X 2 electrode locations (original and shifted)) using two-way repeated ANOVA. Fisher's transformation was applied to the correlation values to satisfy the normality requirement. For the main effects that reached a significant level, post hoc comparisons were conducted. For the interaction effects that reached a significant level, the post hoc pairwise comparison was conducted to break down the interaction into simple effects. Tukey's honestly significant difference test was used for all post hoc tests. The significant level was set at $\alpha = 0.05$.

For the simulated noise results, correlation and NRMSE values were averaged for each subject, joint, and level of simulated noise for each decoder. For each decoder, the mean correlation and NRMSE were linearly fit as a function of level of simulated noise via a least squares method. The slopes of the fitted lines were used as a metric to indicate how quickly performance decreased as the level of noise increased. Faster decreases in performance were indicated by larger magnitudes of negative slopes for correlation values and larger magnitudes of positive slopes for NRMSE values. The slope for each decoder for each joint was compared using one-way repeated measures ANOVA with decoder type as the independent variable. Tukey's honestly significant difference test was used to determine significant differences. The significant level was set at $\alpha = 0.05$.

2) Virtual Posture Matching Test: The average task completion percentage and mean absolute jerk across all trials and the average task duration, number of overshoots, and normalized path length for each completed posture for the N2M2 and NN decoders were compared using a paired 2-sample t-test. Differences were considered significant for $p < 0.05$.

3) Smoothness of Estimated Joint Positions: The average mean absolute jerk for each decoder was compared using one-way repeated measures ANOVA with decoder type as the independent variable. A Tukey test was used to determine significant differences. Differences were considered significant for $p < 0.05$.

4) Prosthetic Device Tests: For the prosthetic device tests, the average performance metric for each test (e.g., number of blocks moved or time taken to flip all cards) across all subjects and trials was calculated to give an idea of the typical ability of the N2M2 decoder for performing some ADLs.

III. Results

In this section, we quantify the robustness of each decoder for ND subject data by first establishing a baseline for comparisons by testing with data similar to the training data (original posture, original electrode locations, and no simulated noise). Example representative plots of simultaneously measured and estimated wrist and MCP joint angles from a section of a baseline trial for an ND subject are shown in Fig. 7. Similar representative plots

TABLE IV
AVERAGE PEARSON'S CORRELATION COEFFICIENT AND NRMSE BETWEEN ESTIMATED AND MEASURED JOINT ANGLES OF TRIALS COMPLETED BY THE TRANSRADIAL AMPUTEE SUBJECT FOR EACH DECODER

Pearson's Correlation Coefficient (r)				Normalized Root Mean Square Error (NRMSE)			
N2M2	MM	NN	MLP	N2M2	MM	NN	MLP
0.88±0.07	0.82±0.12	0.87±0.14	0.65±0.08	0.15±0.04	0.20±0.07	0.15±0.06	0.22±0.02

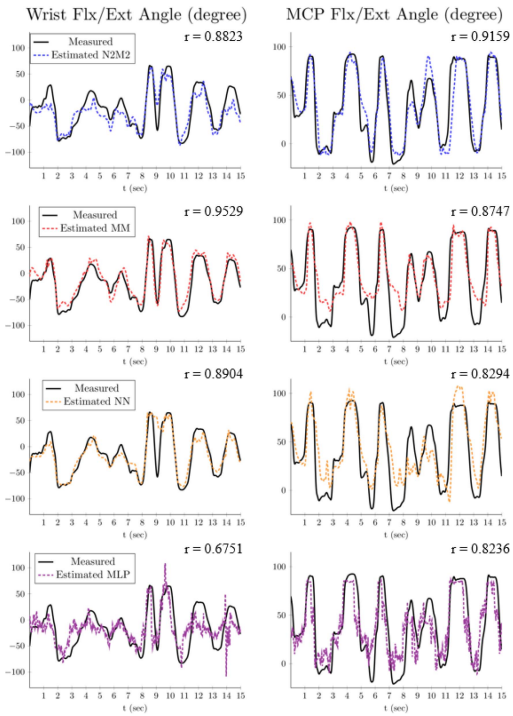

Fig. 7. Representative plots of simultaneous wrist (left) and MCP (right) joint angles estimated by the N2M2 (blue), MM (red), NN (orange), and MLP (purple) decoders for a trial completed by a non-disabled subject with self-selected movement velocities. Measured joint angles are represented by the black lines.

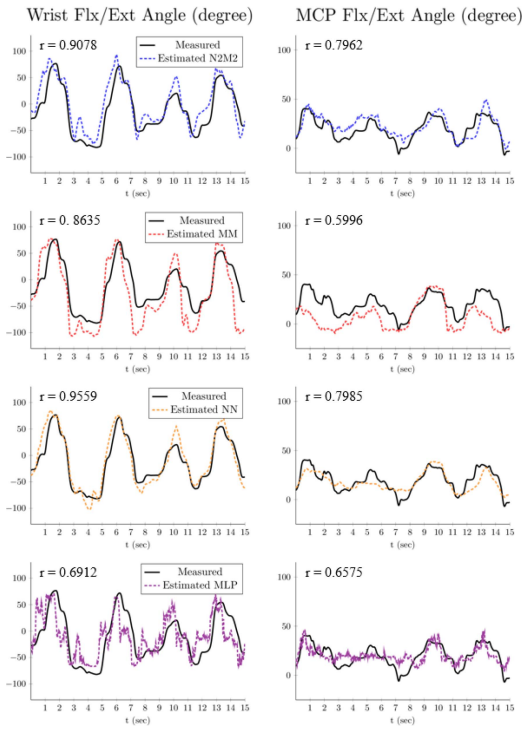

Fig. 8. Representative plots of simultaneous wrist (left) and MCP (right) joint angles estimated by the N2M2 (blue), MM (red), NN (orange), and MLP (purple)decoders for a trial completed by the transradial amputee subject with self-selected movement velocities. Measured joint angles are represented by the black lines.

for a trial completed by the TRA subject are shown in Fig. 8 and the average performance achieved by each decoder for trials completed by the TRA subject are summarized in Table IV. All results are reported as the mean ± standard deviation unless stated otherwise.

1) Varied Posture: The respective correlation values for the N2M2, MM, NN, and MLP decoders were 0.86 ± 0.10, 0.88 ± 0.10, 0.89 ± 0.09, and 0.69 ± 0.12 for the original posture, 0.76 ± 0.17, 0.78 ± 0.15, 0.78 ± 0.16, and 0.56 ± 0.17 for the pronated posture, and 0.80 ± 0.17, 0.82 ± 0.15, 0.82 ± 0.15, and 0.59 ± 0.14 for the raised posture (Fig. 9). Two-way ANOVA revealed no significant interaction ($p = 0.22$). The main effects of both variables were found to be significant ($p < 0.001$). The Tukey test determined that the decoders performed better in the original posture when compared to either the pronated or raised postures ($p < 0.009$), but the decoders performed similarly in the pronated and raised postures ($p = 0.34$). Additionally, across all postures, correlation values of the N2M2, MM, and NN decoders were not significantly different ($p > 0.27$). However, it was found that the correlation values of the MLP decoder were significantly lower than each of the other 3 decoders ($p < 0.001$).

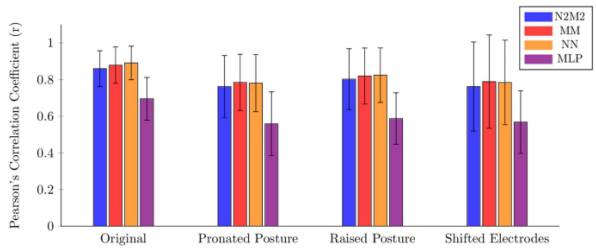

Fig. 9. Average Pearson's correlation coefficient (r) between estimated and measured joint angles of the N2M2 (blue), MM (red), NN (orange), and MLP (purple) decoders for each of the 3 postures and shifted electrode locations. Error bars represent standard deviation.

2) Shifted Electrodes: The respective correlation values for the N2M2, MM, NN, and MLP decoders were 0.86 ± 0.10, 0.88 ± 0.10, 0.89 ± 0.09, and 0.69 ± 0.12 for the original electrode locations and 0.76 ± 0.24, 0.79 ± 0.25, 0.78 ± 0.23, and 0.57 ± 0.17 for the shifted electrode locations (Fig. 9). Two-way ANOVA revealed no significant interaction ($p = 0.19$). Significance was determined for both decoder type and electrode

location ($p < 0.006$). The Tukey test determined that the decoder performed better for original electrode locations when compared to shifted electrode locations ($p = 0.005$). Additionally, no significant differences were found between the correlation values of the N2M2, MM, and NN decoders ($p > 0.33$). However, it was found that the correlation values of the MLP decoder were significantly lower than each of the other 3 decoders ($p < 0.001$).

3) Simulated Noise: The average values of the slopes of the lines fitted to the average correlation values across all subjects for the N2M2, MM, NN, and MLP decoders were $-8.63 \pm 10.50\ V^{-1}$, $-6.33 \pm 6.99\ V^{-1}$, $-18.80 \pm 8.85\ V^{-1}$, and $-10.34 \pm 10.59\ V^{-1}$ respectively for the wrist joint and $-8.63 \pm 9.19\ V^{-1}$, $-14.46 \pm 14.72\ V^{-1}$, $-43.96 \pm 25.62\ V^{-1}$, and $-13.50 \pm 6.21\ V^{-1}$ respectively for the MCP joint. One-way ANOVA revealed significance for the main effect of decoder type in the cases of both the wrist ($p = 0.005$) and MCP joint ($p < 0.001$). For the wrist joint, the Tukey test revealed no significant differences between the slopes of lines fitted to average correlation values for the N2M2, MM, and MLP decoders ($p > 0.77$). Additionally, no significant difference was found between the slopes for the NN and MLP decoder ($p = 0.11$), but it was found that the slopes of the NN decoder had significantly larger magnitudes than the slopes of either the N2M2 or MM decoders ($p < 0.048$). For the MCP joint, the Tukey test revealed no significant differences between the slopes for the N2M2, MM, and MLP decoders ($p > 0.40$). However, the magnitudes of the slopes for the NN decoder were found to be significantly larger than those of each of the other 3 decoders ($p < 0.027$).

The average values of the slopes of the lines fitted to the average NRMSE values across all subjects for the N2M2, MM, NN, and MLP decoders were $7.25 \pm 7.18\ V^{-1}$, $14.31 \pm 15.20\ V^{-1}$, $16.63 \pm 11.08\ V^{-1}$, and $3.80 \pm 3.16\ V^{-1}$ respectively for the wrist joint and $6.39 \pm 7.54\ V^{-1}$, $30.49 \pm 20.56\ V^{-1}$, $25.18 \pm 13.61\ V^{-1}$, and $5.16 \pm 3.19\ V^{-1}$ respectively for the MCP joint. One-way ANOVA revealed significance for the main effect of decoder type in the cases of both the wrist ($p = 0.026$) and MCP joint ($p < 0.001$). For the wrist joint, the Tukey test revealed that the slopes for the NN decoder were significantly larger than the slopes of the MLP decoder ($p = 0.031$). However, no significant differences were found between the slopes of any other pair of decoders ($p > 0.14$). For the MCP joint, there were no significant differences found between the slopes for the N2M2 and MLP decoders ($p = 0.94$) or between the slopes for the MM and NN decoders ($p = 0.73$). However, it was found that the slopes of either the MM or NN decoder were significantly larger than the slopes of either the N2M2 or MLP decoder ($p < 0.031$).

Lines were additionally fitted to the average metrics for both joints across all subjects and are shown in Fig. 10.

4) Smoothness of Estimated Joint Positions: The average mean absolute jerk for the offline estimations made by the N2M2, MM, NN, and MLP decoders were 7.77e4 ± 4.67e4 degrees/s^3, 1.05e4 ± 5.45e3 degrees/s^3, 3.53e5 ± 4.67e5 degrees/s^3, and 5.43e6 ± 1.62e6 degrees/s^3 respectively (Fig. 11(a)). One-way ANOVA revealed significance for the main effect of decoder type ($p < 0.001$). The Tukey test revealed that the MM decoder had significantly lower mean absolute jerk than each of the other 3 decoders ($p < 0.001$), the N2M2 decoder had significantly lower mean absolute jerk than the NN or MLP decoders ($p < 0.001$), and the NN decoder had significantly lower mean absolute jerk than the MLP decoder ($p < 0.001$).

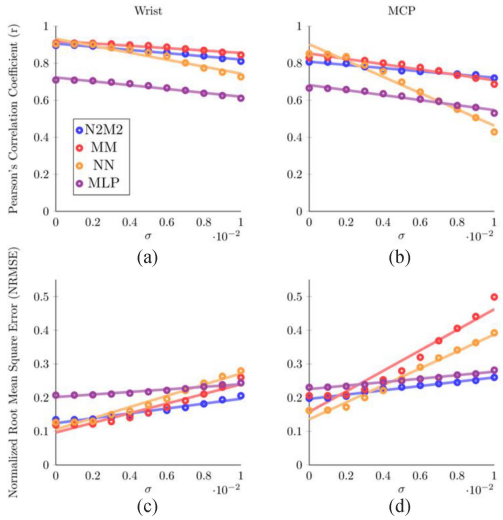

Fig. 10. Average points and fitted lines for the Pearson's correlation coefficient (r) (top) and NRMSE (bottom) between estimated and measured wrist (left) and MCP (right) joint angles of the N2M2 (blue), MM (red), NN (orange), and MLP (purple) decoders for EMG data with added Gaussian noise with increasing standard deviation (σ).

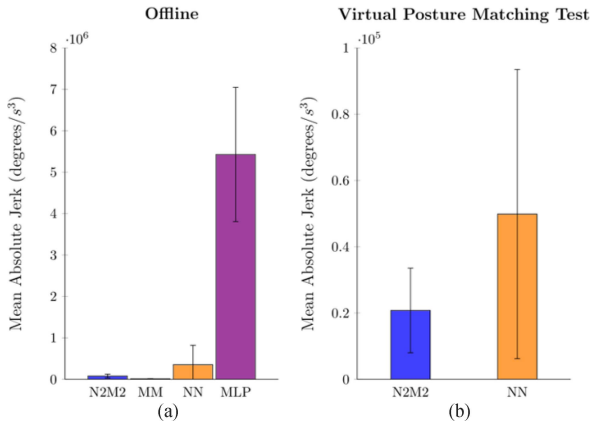

Fig. 11. The average mean absolute jerk for joint angles estimated offline (excluding simulated noise cases) (a) and during the Virtual Posture Matching Test (b) for each decoder. Lower values indicate smoother estimated position trajectories. Error bars represent standard deviation.

A. Real-Time Control

1) Virtual Posture Matching Test: For the N2M2 decoder, the task completion percentage, task duration, normalized path length, and number of overshoots were 99.56 ± 2.22%, 9.18 ± 7.80 s, 5.70 ± 6.44, and 3.23 ± 2.91 respectively. For the NN decoder the task completion percentage, task duration, normalized path length, and number of overshoots were 84.89 ± 13.56%, 10.71 ± 10.63 s, 7.32 ± 8.66, 4.18 ± 4.26 respectively. The average mean absolute jerk for the N2M2 and NN decoders were 2.08e4 ± 1.28e4 degrees/s^3 and 4.98e4 ± 4.36e4 degrees/s^3 respectively. Results were found to be significantly different between the 2 decoders for task completion percentage

TABLE V
AVERAGE PERFORMANCE METRICS FOR THE REAL-TIME TESTS WITH THE PROSTHETIC DEVICE

Test	Performance Metric Used	Average Performance Metric Value
Box and Blocks	Number of Blocks Moved	10.84±2.51
Modified Page Turning	Task Completion Time (s)	47.23±16.03
Shelf	Number of Blocks Moved	10.60±2.94

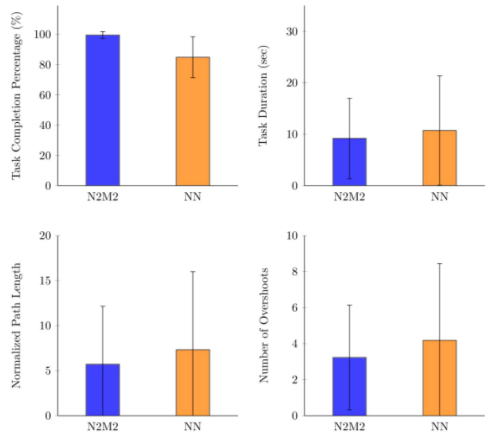

Fig. 12. Average task completion percentage, task duration, normalized path length, and number of overshoots achieved by subjects using the N2M2 and NN decoders. Error bars represent standard deviation.

($p < 0.001$), normalized path length ($p = 0.030$), number of overshoots ($p = 0.009$), and mean absolute jerk ($p < 0.001$). Task duration was slightly lower for the N2M2 decoder than the NN decoder but was not found to be significantly different ($p = 0.092$). The values of task completion percentage, task duration, normalized path length, and NO are summarized in Fig. 12 and mean absolute value is summarized in Fig. 11(b). Additionally, all 5 subjects indicated that they preferred the N2M2 decoder.

2) Prosthetic Device Tests: The number of blocks moved in the Box and Blocks Test, time taken to complete the Modified Page Turning Test, and number of blocks moved in the Shelf Test were 10.84 ± 2.51, 47.23 ± 16.03 s, and 10.60 ± 2.94 respectively when averaged across all subjects and trials. These results are summarized in Table V. Examples of the performance achieved by the N2M2 decoder for each test is shown in the attached video.

IV. DISCUSSION

In this study, we developed a novel EMG-based decoding algorithm that is RL-trained and can predict continuous joint kinematics from non-disabled and amputee subjects. This decoder is leveraged by the benefit of both machine learning and musculoskeletal model-based decoding concepts. Our algorithm follows the human limb motion production process, in which EMG signal magnitude represents the intended force/torque rather than joint motion. When compared to the NN decoder, our system yielded significantly higher online performance for the posture matching task. Additionally, our developed EMG-based NMI can estimate both virtual joint torque and joint positions continuously based on EMG signals. Although we did not directly use the virtual joint torque for prosthesis control, this study introduces the possibility of using virtual joint torque in real-time for future applications.

The results suggested that using a recurrent structure for ANN-based EMG decoding can potentially provide better joint kinematics estimations. In the recurrent structure of ANN, the estimated joint kinematics for one timestep are fed back as inputs to the ANNs in the following timestep. Such a strategy, adopted by N2M2 and NN decoders, showed better offline performance than the MLP decoder, which estimated joint angles in an open-loop manner. Specifically, the network structure of the MLP decoder was identical to that of the NN decoder with the exception of the feedback loop. The NN decoder, however, consistently outperformed the MLP in offline evaluation for accurate estimations of joint kinematics across various testing scenarios (including varied electrode locations and arm positions). We believe the performance increase observed from the MLP to NN decoder through introducing a feedback loop is largely because providing the last estimated joint angle via the feedback loop introduces the ability to train an ANN not to make large, erroneous changes in estimated joint angles over a short timestep. Similarly, the N2M2 decoder also produced significantly better kinematic estimations than the MLP decoder in all offline testing conditions. From a dynamic system point of view, the system output depends on both external inputs as well as the current system state. Hence, the input joint position enables better estimations of virtual joint torque by the ANN for forward dynamic simulation.

A lowpass filtering effect in an EMG decoder, such as the one introduced by the forward dynamics model, will likely result in more accurate estimations of joint positions regardless of minor variations in the input EMG signals. This is evidenced by our analysis of offline performance that revealed that both the N2M2 and MM decoders were less sensitive to noise than NN decoder in terms of correlation of joint positions (Fig. 10). This is likely because the forward dynamics model included in the N2M2 and MM decoders works to mimic the dynamics of the wrist and MCP joints of a healthy, intact limb. In general, the estimated joint angles output from the model appeared to follow a smooth, continuous trajectory as a result of simulated damping and inertia properties of the forward dynamics model which resulted in a lowpass filtering effect. This was confirmed by the comparison of the smoothness of estimated joint positions which revealed that in terms of mean absolute jerk, the decoders with forward dynamics models (i.e., N2M2 and MM decoders) produced smoother trajectories than either the pure machine learning decoders (i.e., NN and MLP decoders) (Fig. 11). This lowpass filtering and natural smoothing effect likely helped to improve sensitivity to any high frequencies in the input and prevent the jerkiness of a noisy input from propagating to the output. While no additional lowpass filters were included in the

NN or MLP decoders for this study, any future work should consider adding an extra lowpass filtering step and can determine if higher performance and robustness to variations in input EMG signals are achievable. Additionally, it was found that when noise was added to input EMG signals, the values of NRMSE, specifically for the MCP joint angles, increased at a significantly higher rate for the MM decoder when compared to the N2M2 decoder. Poor MCP joint angle decoding accuracy with the same musculoskeletal model has been noted in a previous study, potentially as a result of inexact electrode placement and EMG crosstalk [22]. Future work can be conducted to investigate the specific differences between the N2M2 and MM decoders in terms of sensitivity to electrode placement during the initial training data collection and EMG crosstalk.

We predicted that the higher robustness and smoothness of the N2M2 decoder would be beneficial for efficiently completing dynamic online tasks. The Virtual Posture Matching Test, for instance, was completed in a session at least several days after the initial training data collection session used to calibrate each decoder. Despite any similarities in the average correlation and NRMSE calculated offline, we found that the N2M2 decoder had significantly higher performance and was more preferred by subjects. It is likely that the N2M2 decoder was more robust to any changes in EMG signals between the 2 sessions (e.g., differences in skin impedance, signal to noise ratio of EMG signals, levels of muscle fatigue, ect.) as suggested by the results from our analysis of performance with noisy EMG signals (Fig. 10). For another example, our N2M2 can be applied to control of a 2DOF prosthesis, which enables the users to perform physical functional tasks. This result also indicated that N2M2 was robust as the prosthesis attached to the human user leads to external weight changes to the arm. The evidence implied that it is likely that a musculoskeletal modeling approach such as our N2M2 decoder will work well after only one system calibration session while pure machine learning approaches will be subject to frequent and inconvenient system recalibrations. Additionally, the smoothness of the decoder allowed subjects to more easily maintain constant joint positions necessary for completing each target posture. The moving average filters did help to improve the smoothness of joint position estimations made by both the N2M2 and NN decoders as seen by the drop in average mean absolute jerk from the offline analysis to the Virtual Posture Matching Test (Fig. 11). However, the outputs of the higher-performing N2M2 decoder remained significantly less jerky than the outputs of the NN decoder. Thus, the smoothness of the output of a decoder may be more desirable for tasks that require fine motor control. Additionally, other future studies can consider offline metrics such as mean absolute jerk to estimate the level of smoothness or jerkiness that can be expected during online tasks.

Several limitations were identified in this study. First, the initial RL training of the N2M2 decoder took approximately 8 hours as a result of the much larger ANN sizes and extra computation time needed for the forward dynamics simulation. Contrarily, the NN and MLP decoders can be trained within minutes. Although N2M2 does not require frequent retraining across days, further reducing the computational complexity of the RL training process is needed. One potential solution is to leverage learning transfer to accelerate the learning process. Second, our approach to filtering estimated joint angles in real-time included only a moving average filter. As discussed previously, the N2M2 decoder benefits from the lowpass characteristics of the forward dynamics model that the NN decoder does not have. It may be beneficial to investigate the effect of additional lowpass filtering at the input of the NN decoder as a method of reducing remaining high-frequency noise in the signals which can cause unexpected behavior. Furthermore, future work can consider alternate filtering approaches, including finite impulse response and infinite impulse response filters, to reduce jerkiness and improve functional task performance. Third, our study was limited in the sample size. More human subjects should be included in the future work to systematically evaluate the benefit of our N2M2 decoder to amputee patients. Fourth, all patterned movements were completed by subjects at a single movement frequency. Future work should consider including movement frequencies across a range of reasonable values to improve and test robustness to those frequencies. Finally, one feature of N2M2 that has not been explored in this study is the application of the estimated virtual joint torque. Future research can focus on exploring the feasibility of applying the virtual torque for grasping force control in prosthesis or feeding back virtual joint torque to users as an artificial proprioception for improved robotic arm control.

V. Conclusion

In this study, we introduced a novel EMG-based decoder called N2M2 that harnessed machine learning within the known physiology of neuromusculoskeletal system in humans. We compared our N2M2 decoder to two other block-box ANN-based decoders, with and without recurrent structures, as well as a musculoskeletal model. Our results suggest that using a recurrent ANN as well as lowpass filtering similar to the effects introduced by our forward dynamics model in EMG decoder design was important to estimating joint motion both offline and online. Further work should be done in determining the specific differences between the N2M2 and MM decoder in terms of sensitivity to exact electrode placement when collecting initial training data and EMG crosstalk. Finally, we demonstrated the capabilities for real-time control of a prosthetic hand with different functional tasks. These promising results implied that our EMG-based NMI was feasible for reliable control of a transradial prosthetic device and potentially other applications in human-machine systems.

References

[1] S. Goto et al., "Development of hands-free remote operation system for a mobile robot using EOG and EMG," *Electron. Commun. Jpn.,* vol. 100, no. 10, pp. 38–47, 2017.

[2] S. Bisi et al., "Development of an EMG-controlled mobile robot," *Robotics*, vol. 7, no. 3, 2018, Art. no. 36.

[3] A. Gaggioli et al., "A myoelectric-controlled virtual hand for the assessment and treatment of phantom limb pain in trans-radial upper extremity amputees: A research protocol," *Stud. Health Technol. Inform.,* vol. 154, 2010, Art. no. 220.

[4] L. Liu et al., "Development of an EMG-ACC-based upper limb rehabilitation training system," *IEEE Trans. Neural Syst. Rehabil. Eng.,* vol. 25, no. 3, pp. 244–253, Mar. 2017.

[5] P. Geethanjali, "Myoelectric control of prosthetic hands: State-of-the-art review," *Med Devices*, vol. 9, pp. 247–255, 2016.

[6] N. Parajuli et al., "Real-time EMG based pattern recognition control for hand prostheses: A review on existing methods, challenges and future implementation," *Sensors*, vol. 19, no. 20, 2019, Art. no. 4596.

[7] L. Resnik et al., "Evaluation of EMG pattern recognition for upper limb prosthesis control: A case study in comparison with direct myoelectric control," *J. Neuroengineering Rehabil.,* vol. 15, no. 1, 2018, Art. no. 23.

[8] M. M. White et al., "Usability comparison of conventional direct control versus pattern recognition control of transradial prostheses," *IEEE Trans. Hum.-Mach. Syst.,* vol. 47, no. 6, pp. 1146–1157, Dec. 2017.

[9] A. A. Adewuyi, L. J. Hargrove, and T. A. Kuiken, "An analysis of intrinsic and extrinsic hand muscle EMG for improved pattern recognition control," *IEEE Trans. Neural Syst. Rehabil. Eng.,* vol. 24, no. 4, pp. 485–494, Apr. 2016.

[10] K. Englehart and B. Hudgins, "A robust, real-time control scheme for multifunction myoelectric control," *IEEE Trans. Biomed. Eng.,* vol. 50, no. 7, pp. 848–854, Jul. 2003.

[11] A. Waris et al., "Multiday evaluation of techniques for EMG-based classification of hand motions," *IEEE J. Biomed. Health Inform.,* vol. 23, no. 4, pp. 1526–1534, Jul. 2019.

[12] X. Zhang and H. Huang, "A real-time, practical sensor fault-tolerant module for robust EMG pattern recognition," *J. Neuroengineering Rehabil.,* vol. 12, no. 1, pp. 1–16, 2015.

[13] M. Ortiz-Catalan, B. Hakansson, and R. Branemark, "Real-time and simultaneous control of artificial limbs based on pattern recognition algorithms," *IEEE Trans. Neural Syst. Rehabil. Eng.,* vol. 22, no. 4, pp. 756–764, Jul. 2014.

[14] L. H. Smith, T. A. Kuiken, and L. J. Hargrove, "Evaluation of linear regression simultaneous myoelectric control using intramuscular EMG," *IEEE Trans. Biomed. Eng.,* vol. 63, no. 4, pp. 737–746, Apr. 2016.

[15] J. M. Hahne et al., "Linear and nonlinear regression techniques for simultaneous and proportional myoelectric control," *IEEE Trans. Neural Syst. Rehabil. Eng.,* vol. 22, no. 2, pp. 269–279, Mar. 2014.

[16] L. Pan, D. L. Crouch, and H. Huang, "Comparing EMG-based human-machine interfaces for estimating continuous, coordinated movements," *IEEE Trans. Neural Syst. Rehabil. Eng.,* vol. 27, no. 10, pp. 2145–2154, Oct. 2019.

[17] D. Farina et al., "The extraction of neural information from the surface EMG for the control of upper-limb prostheses: Emerging avenues and challenges," *IEEE Trans. Neural Syst. Rehabil. Eng.,* vol. 22, no. 4, pp. 797–809, Jul. 2014.

[18] S. Muceli and D. Farina, "Simultaneous and proportional estimation of hand kinematics from EMG during mirrored movements at multiple degrees-of-freedom," *IEEE Trans. Neural Syst. Rehabil. Eng.*, vol. 20, no. 3, pp. 371–378, May 2012.

[19] J. G. Ngeo, T. Tamei, and T. Shibata, "Continuous and simultaneous estimation of finger kinematics using inputs from an EMG-to-muscle activation model," *J. Neuroengineering Rehabil.,* vol. 11, 2014, Art. no. 122.

[20] N. Jiang et al., "Effect of arm position on the prediction of kinematics from EMG in amputees," *Med. Biol. Eng. Comput.,* vol. 51, no. 1-2, pp. 143–151, 2013.

[21] P. Xia, J. Hu, and Y. Peng, "EMG-based estimation of limb movement using deep learning with recurrent convolutional neural networks," *Artif. Organs,* vol. 42, no. 5, pp. E67–E77, 2018.

[22] D. L. Crouch and H. Huang, "Lumped-parameter electromyogram-driven musculoskeletal hand model: A potential platform for real-time prosthesis control," *J. Biomech.,* vol. 49, no. 16, pp. 3901–3907, 2016.

[23] R. Heine, K. Manal, and T. S. Buchanan, "Using hill-type muscle models and EMG data in a forward dynamic analysis of joint moment: Evaluation of critical parameters," *J. Mechanics Med. Biol.,* vol. 3, no. 2, pp. 169–186, 2003.

[24] L. Pan, D. L. Crouch, and H. Huang, "Myoelectric control based on a generic musculoskeletal model: Toward a multi-user neural-machine interface," *IEEE Trans. Neural Syst. Rehabil. Eng.,* vol. 26, no. 7, pp. 1435–1442, Jul. 2018.

[25] L. Pan, D. Crouch, and H. Huang, "Musculoskeletal model for simultaneous and proportional control of 3-DOF hand and wrist movements from EMG signals," in *Proc. 8th Int. IEEE/EMBS Conf. Neural Eng.*, 2017, pp. 325–328.

[26] M. Sartori, D. G. Llyod, and D. Farina, "Neural data-driven musculoskeletal modeling for personalized neurorehabilitation technologies," *IEEE Trans. Biomed. Eng.,* vol. 63, no. 5, pp. 879–893, May 2016.

[27] D. G. Lloyd and T. F. Besier, "An EMG-driven musculoskeletal model to estimate muscle forces and knee joint moments in vivo," *J. Biomech.,* vol. 36, no. 6, pp. 765–776, 2003.

[28] M. Sartori et al., "Robust simultaneous myoelectric control of multiple degrees of freedom in wrist-hand prostheses by real-time neuromusculoskeletal modeling," *J. Neural Eng.,* vol. 15, no. 6, 2018, Art. no. 066026.

[29] F. E. Zajac, "Muscle and tendon: Properties, models, scaling, and application to biomechanics and motor control," *Crit. Rev. Biomed. Eng.,* vol. 17, no. 4, 1989, Art. no. 359.

[30] K. Arulkumaran et al., "Deep reinforcement learning: A brief survey," *IEEE Signal Process. Mag.*, vol. 34, no. 6, pp. 26–38, Nov. 2017.

[31] J. Berman, R. Hinson, and H. Huang, "Comparing reinforcement learning agents and supervised learning neural networks for EMG-based decoding of continuous movements," in *Proc. 43rd Annu. Int. Conf. IEEE Eng. Med. Biol. Soc.*, 2021, pp. 6297–6300.

[32] J. Liu et al., "EMG-based continuous and simultaneous estimation of arm kinematics in able-bodied individuals and stroke survivors," *Front. Neurosci.,* vol. 11, 2017, Art. no. 480.

[33] T. P. Lillicrap et al., "Continuous control with deep reinforcement learning," in *Proc. 4th Int. Conf. Learn. Representations*, 2016, Art. no. 10.

[34] W. Wu, K. R. Saul, and H. Huang, "Using reinforcement learning to estimate human joint moments from electromyography or joint kinematics: An alternative solution to musculoskeletal-based biomechanics," *J. Biomechanical Eng.,* vol. 143, no. 4, 2021, Art. no. 044502.

[35] N. Hogan and D. Sternad, "Sensitivity of smoothness measures to movement duration, amplitude, and arrests," *J. Motor Behav.,* vol. 41, no. 6, pp. 529–534, 2009.

[36] H.-L. Teulings et al., "Parkinsonism reduces coordination of fingers, wrist, and arm in fine motor control," *Exp. Neurol.,* vol. 146, no. 1, pp. 159–170, 1997.

[37] A. M. Simon et al., "Target achievement control test: Evaluating real-time myoelectric pattern-recognition control of multifunctional upper-limb prostheses," *J. Rehabil. Res. Develop.,* vol. 48, no. 6, 2011, Art. no. 619.

[38] D. L. Crouch et al., "Comparing surface and intramuscular electromyography for simultaneous and proportional control based on a musculoskeletal model: A pilot study," *IEEE Trans. Neural Syst. Rehabil. Eng.,* vol. 26, no. 9, pp. 1735–1744, Sep. 2018.

[39] L. Pan, A. Harmody, and H. Huang, "A reliable multi-user EMG interface based on a generic-musculoskeletal model against loading weight changes," in *Proc. 40th Annu. Int. Conf. IEEE Eng. Med. Biol. Soc.*, 2018, pp. 2104–2107.

[40] S. H. Chung, D. L. Crouch, and H. H. Huang, "Effects of output speed threshold on real-time continuous emg human-machine interface control," in *Proc. IEEE Int. Conf. Syst., Man, Cybern.*, 2017, pp. 1375–1380.

[41] V. Mathiowetz et al., "Adult norms for the box and block test of manual dexterity," *Amer. J. Occup. Ther.,* vol. 39, no. 6, pp. 386–391, 1985.

[42] C. M. Light, P. H. Chappell, and P. J. Kyberd, "Establishing a standardized clinical assessment tool of pathologic and prosthetic hand function: Normative data, reliability, and validity," *Arch. Phys. Med. Rehabil.,* vol. 83, no. 6, pp. 776–783, 2002.